Photon-tissue interaction model enables quantitative optical analysis of human pancreatic tissues

Robert H. Wilson,[1] Malavika Chandra[1,2], Leng-Chun Chen[2], William R. Lloyd[2], James Scheiman[3,4], Diane Simeone[4,5], Julianne Purdy[6], Barbara McKenna[6], and Mary-Ann Mycek[1,2,4,*]

[1]*Applied Physics Program, University of Michigan, Ann Arbor, MI 48109-1040, USA*
[2]*Department of Biomedical Engineering, University of Michigan, Ann Arbor, MI 48109-2099, USA*
[3]*Department of Internal Medicine, University of Michigan, Ann Arbor, MI 48109-0362, USA*
[4]*Comprehensive Cancer Center, University of Michigan, Ann Arbor, MI 48109-0944, USA*
[5]*Department of Surgery, University of Michigan, Ann Arbor, MI 48109-5331, USA*
[6]*Department of Pathology, University of Michigan, Ann Arbor, MI 48109-0602, USA*
**mycek@umich.edu*

Abstract: A photon-tissue interaction (PTI) model was developed and employed to analyze 96 pairs of reflectance and fluorescence spectra from freshly excised human pancreatic tissues. For each pair of spectra, the PTI model extracted a cellular nuclear size parameter from the measured reflectance, and the relative contributions of extracellular and intracellular fluorophores to the intrinsic fluorescence. The results suggest that reflectance and fluorescence spectroscopies have the potential to quantitatively distinguish among pancreatic tissue types, including normal pancreatic tissue, pancreatitis, and pancreatic adenocarcinoma.

OCIS codes: (170.4580) Optical diagnostics for medicine; (170.6510) Spectroscopy, tissue diagnostics; (170.3660) Light propagation in tissues.

References and links

1. "Cancer Facts & Figures 2010," (American Cancer Society, 2010), *www.cancer.org*.
2. A. Fritscher-Ravens, L. Brand, W. T. Knöfel, C. Bobrowski, T. Topalidis, F. Thonke, A. de Werth, and N. Soehendra, "Comparison of endoscopic ultrasound-guided fine needle aspiration for focal pancreatic lesions in patients with normal parenchyma and chronic pancreatitis," Am. J. Gastroenterol. **97**(11), 2768–2775 (2002).
3. W. Hartwig, L. Schneider, M. K. Diener, F. Bergmann, M. W. Büchler, and J. Werner, "Preoperative tissue diagnosis for tumours of the pancreas," Br. J. Surg. **96**(1), 5–20 (2009).
4. S. C. Abraham, R. E. Wilentz, C. J. Yeo, T. A. Sohn, J. L. Cameron, J. K. Boitnott, and R. H. Hruban, "Pancreaticoduodenectomy (Whipple resections) in patients without malignancy: are they all 'chronic pancreatitis'?" Am. J. Surg. Pathol. **27**(1), 110–120 (2003).
5. Z. Volynskaya, A. S. Haka, K. L. Bechtel, M. Fitzmaurice, R. Shenk, N. Wang, J. Nazemi, R. R. Dasari, and M. S. Feld, "Diagnosing breast cancer using diffuse reflectance spectroscopy and intrinsic fluorescence spectroscopy," J. Biomed. Opt. **13**(2), 024012 (2008).
6. G. Zonios, L. T. Perelman, V. Backman, R. Manoharan, M. Fitzmaurice, J. Van Dam, and M. S. Feld, "Diffuse reflectance spectroscopy of human adenomatous colon polyps *in vivo*," Appl. Opt. **38**(31), 6628–6637 (1999).
7. S. K. Chang, N. Marin, M. Follen, and R. Richards-Kortum, "Model-based analysis of clinical fluorescence spectroscopy for *in vivo* detection of cervical intraepithelial dysplasia," J. Biomed. Opt. **11**(2), 024008 (2006).
8. I. Georgakoudi, and M. S. Feld, "The combined use of fluorescence, reflectance, and light-scattering spectroscopy for evaluating dysplasia in Barrett's esophagus," Gastrointest. Endosc. Clin. N. Am. **14**(3), 519–537, ix (2004).
9. P. A. Testoni, B. Mangiavillano, L. Albarello, P. G. Arcidiacono, A. Mariani, E. Masci, and C. Doglioni, "Optical coherence tomography to detect epithelial lesions of the main pancreatic duct: an *Ex Vivo* study," Am. J. Gastroenterol. **100**(12), 2777–2783 (2005).
10. P. A. Testoni, A. Mariani, B. Mangiavillano, P. G. Arcidiacono, S. Di Pietro, and E. Masci, "Intraductal optical coherence tomography for investigating main pancreatic duct strictures," Am. J. Gastroenterol. **102**(2), 269–274 (2007).

#130269 - $15.00 USD Received 16 Jun 2010; revised 22 Sep 2010; accepted 23 Sep 2010; published 28 Sep 2010

11. V. R. Kondepati, J. Zimmermann, M. Keese, J. Sturm, B. C. Manegold, and J. Backhaus, "Near-infrared fiber optic spectroscopy as a novel diagnostic tool for the detection of pancreatic cancer," J. Biomed. Opt. **10**(5), 054016 (2005).
12. H. Subramanian, P. Pradhan, Y. Liu, I. R. Capoglu, J. D. Rogers, H. K. Roy, R. E. Brand, and V. Backman, "Partial-wave microscopic spectroscopy detects subwavelength refractive index fluctuations: an application to cancer diagnosis," Opt. Lett. **34**(4), 518–520 (2009).
13. M. Chandra, J. Scheiman, D. Heidt, D. Simeone, B. McKenna, and M.-A. Mycek, "Probing pancreatic disease using tissue optical spectroscopy," J. Biomed. Opt. **12**(6), 060501 (2007).
14. M. Chandra, J. Scheiman, D. Simeone, B. McKenna, J. Purdy, and M.-A. Mycek, "Spectral areas and ratios classifier algorithm for pancreatic tissue classification using optical spectroscopy," J. Biomed. Opt. **15**(1), 010514 (2010).
15. R. H. Wilson, M. Chandra, J. Scheiman, D. Simeone, B. McKenna, J. Purdy, and M. A. Mycek, "Optical spectroscopy detects histological hallmarks of pancreatic cancer," Opt. Express **17**(20), 17502–17516 (2009).
16. M. Chandra, K. Vishwanath, G. D. Fichter, E. Liao, S. J. Hollister, and M.-A. Mycek, "Quantitative molecular sensing in biological tissues: an approach to non-invasive optical characterization," Opt. Express **14**(13), 6157–6171 (2006).
17. J. D. Pitts, and M.-A. Mycek, "Design and development of a rapid acquisition laser-based fluorometer with simultaneous spectral and temporal resolution," Rev. Sci. Instrum. **72**(7), 3061–3072 (2001).
18. R. Reif, M. S. Amorosino, K. W. Calabro, O. A'Amar, S. K. Singh, and I. J. Bigio, "Analysis of changes in reflectance measurements on biological tissues subjected to different probe pressures," J. Biomed. Opt. **13**(1), 010502 (2008).
19. T. Imamura, H. Iguchi, T. Manabe, G. Ohshio, T. Yoshimura, Z. H. Wang, H. Suwa, S. Ishigami, and M. Imamura, "Quantitative analysis of collagen and collagen subtypes I, III, and V in human pancreatic cancer, tumor-associated chronic pancreatitis, and alcoholic chronic pancreatitis," Pancreas **11**(4), 357–364 (1995).
20. B. W. Killough, C. A. Nichols, J. A. Nicholson, and T. S. Gansler, "Diagnosis of pancreatic carcinoma by fine needle aspiration cytology and computerized cytomorphometry," Anal. Quant. Cytol. Histol. **11**(4), 238–242 (1989).
21. A. R. Weger, and J. L. Lindholm, "Discrimination of pancreatic adenocarcinomas from chronic pancreatitis by morphometric analysis," Pathol. Res. Pract. **188**(1-2), 44–48 (1992).
22. F. Lin, and G. Staerkel, "Cytologic criteria for well differentiated adenocarcinoma of the pancreas in fine-needle aspiration biopsy specimens," Cancer **99**(1), 44–50 (2003).
23. P. M. Pour, Y. Konishi, G. Klöppel, and D. S. Longnecker, *Atlas of exocrine pancreatic tumors* (Springer-Verlag, Tokyo, 1994).
24. K. Vishwanath, and M.-A. Mycek, "Do fluorescence decays remitted from tissues accurately reflect intrinsic fluorophore lifetimes?" Opt. Lett. **29**(13), 1512–1514 (2004).
25. K. Vishwanath, and M.-A. Mycek, "Time-resolved photon migration in bi-layered tissue models," Opt. Express **13**(19), 7466–7482 (2005).
26. K. Vishwanath, B. W. Pogue, and M.-A. Mycek, "Quantitative fluorescence lifetime spectroscopy in turbid media: comparison of theoretical, experimental and computational methods," Phys. Med. Biol. **47**(18), 3387–3405 (2002).
27. A. C. Koong, V. K. Mehta, Q. T. Le, G. A. Fisher, D. J. Terris, J. M. Brown, A. J. Bastidas, and M. Vierra, "Pancreatic tumors show high levels of hypoxia," Int. J. Radiat. Oncol. Biol. Phys. **48**(4), 919–922 (2000).
28. S. Kersting, R. Konopke, F. Kersting, A. Volk, M. Distler, H. Bergert, H.-D. Saeger, R. Grützmann, and A. Bunk, "Quantitative perfusion analysis of transabdominal contrast-enhanced ultrasonography of pancreatic masses and carcinomas," Gastroenterology **137**(6), 1903–1911 (2009).
29. J. C. Finlay, and T. H. Foster, "Effect of pigment packaging on diffuse reflectance spectroscopy of samples containing red blood cells," Opt. Lett. **29**(9), 965–967 (2004).

1. Introduction

Pancreatic cancer has a five-year survival rate of only 6% [1], largely because there is currently no reliable method to diagnose the disease in its early stages. Endoscopic ultrasound-guided fine-needle aspiration (EUS-FNA) is currently considered the diagnostic standard for pancreatic cancer diagnosis, but it has a sensitivity of only 54% when the patient also has chronic pancreatitis (pancreatic inflammation), which is frequently the case [2]. For diagnosing cancer in solid lesions of the pancreas, the negative predictive value (true negatives/all negatives) of EUS-FNA has a mean value of 72% and ranges from 16% to 92%, according to a recent meta-analysis of 28 clinical studies [3]. In [3], the authors reported that one of the most common "diagnostic dilemmas" is that of distinguishing malignant masses from inflammatory ones and concluded that EUS-FNA "preoperative biopsy of potentially resectable pancreatic tumours is not generally advisable, as malignancy cannot be ruled out with adequate reliability." Patients who are diagnosed with pancreatic cancer may undergo an

#130269 - $15.00 USD Received 16 Jun 2010; revised 22 Sep 2010; accepted 23 Sep 2010; published 28 Sep 2010

arduous surgical procedure known as a Whipple resection; one study found that fully 9% of Whipple patients were classified as "false positives" [4]. As a result, there is an unmet clinical need for a method that can accurately and reliably detect pancreatic cancer at early stages of development and distinguish it from chronic pancreatitis.

Reflectance and fluorescence spectroscopies have shown potential for clinical cancer detection in tissues including the breast [5], colon [6], cervix [7], and esophagus [8]. However, few studies have used optical methods to detect disease in the human pancreas. Optical interrogation of human pancreatic tissue has been demonstrated with optical coherence tomography [9,10] and near infrared spectroscopy [11]. Partial-wave microscopic spectroscopy has shown promise for detecting cancer-related changes in the nanoarchitecture of human pancreatic cells obtained from archival cytology specimens [12]. Previously, we demonstrated that reflectance and fluorescence spectral features could potentially be employed for human pancreatic cancer detection [13,14]. Further, we developed an empirical photon-tissue interaction (PTI) model to quantitatively link those spectroscopic measurements to histologically known characteristics of malignant and non-malignant human pancreatic tissues [15]. The PTI reflectance model incorporated information about light scattering by cell nuclei and collagen fibers, as well as absorption by oxygenated and deoxygenated hemoglobin. The PTI fluorescence model then corrected fluorescence spectra measured at the same site as the reflectance spectra for absorption and scattering artifacts.

Here, the PTI model was further developed and employed to analyze 96 pairs of reflectance and fluorescence spectra from freshly excised human pancreatic tissues. For each pair of spectra, the PTI model extracted a cellular nuclear size parameter from the measured reflectance, and the relative contributions of extracellular and intracellular fluorophores to the intrinsic fluorescence. The results indicated a statistically significant increase in the nuclear size of adenocarcinoma (relative to both normal pancreatic tissue and chronic pancreatitis) and a statistically significant increase in the extracellular collagen contribution to fluorescence in both adenocarcinoma and chronic pancreatitis (relative to normal pancreatic tissue). This suggests that reflectance and fluorescence spectroscopies have the potential to quantitatively distinguish among pancreatic tissue types, including normal pancreatic tissue, chronic pancreatitis, and pancreatic adenocarcinoma, via biophysical tissue properties extracted from the spectra.

2. Experimental methods

2.1 Instrumentation

At the University of Michigan (U of M), a prototype Reflectance and Fluorescence Lifetime Spectrometer (RFLS), described previously [13,16], was developed to measure reflectance and fluorescence from human pancreatic tissue samples (Fig. 1). Briefly, the RFLS consisted of two light sources: a tungsten halogen lamp (HL 2000FHSA, Ocean Optics, Dunedin, FL) for CW reflectance, and a 355 nm pulsed laser with a 1 KHz repetition rate and a 500 ps pulse width (PNV001525-140, JDS Uniphase, San Jose, CA) for fluorescence excitation. Light from these two sources was directed onto the tissue via two separate optical fibers with core diameter of 600 μm. A third identical fiber was used to detect both the reflectance and fluorescence photons that returned to the surface. These three fibers were incorporated into a custom-made fiber optic probe (Ocean Optics), in which they were arranged in a triangular geometry at the probe's distal end [13]. A portion of the collected signal was directed to time resolved fluorescence measurements (not described here). For wavelength resolved measurements of reflectance and fluorescence, the rest of the detected photons were sent to a spectrograph (MS 125, Oriel Instruments, Stratford, CT) coupled intensified charge coupled device (ICCD) camera (ICCD 2063, Andor Technology, Belfast, Northern Ireland). The detection range of the ICCD was constrained to 340-800 nm by the long-pass filter (shown in Fig. 1) and the spectral grating on the ICCD. Reflectance data from 400 to 700 nm and

#130269 - $15.00 USD Received 16 Jun 2010; revised 22 Sep 2010; accepted 23 Sep 2010; published 28 Sep 2010

fluorescence data from 400 to 638 nm were used in the analysis. At each tissue site, fluorescence and reflectance measurements were made in sequence by using shutters to block the other light source. Each fluorescence (reflectance) measurement had an associated acquisition time of 2 seconds (2.5 seconds).

All measured reflectance and fluorescence spectra were background-corrected and corrected for the instrument response function [17]. Corrected reflectance spectra R/R_o were obtained by background subtraction and then dividing by the reflectance spectrum R_o of the lamp [16]. The lamp spectrum R_o was measured by placing a reflectance standard (SRS-50-010, Labsphere, North Sutton, NH) or a neutral density filter (optical density 0.05) at the distal end of the probe and collecting the lamp light that was reflected from the surface of the reflectance standard. In the reflectance calibration procedure, the fiber probe was placed roughly 6 mm above the reflectance standard. Experiments showed that this distance between the probe and the standard was sufficiently large to prevent the measurements from being sensitive to the lateral spread of light in the standard. Each wavelength-resolved spectrum was normalized to peak intensity.

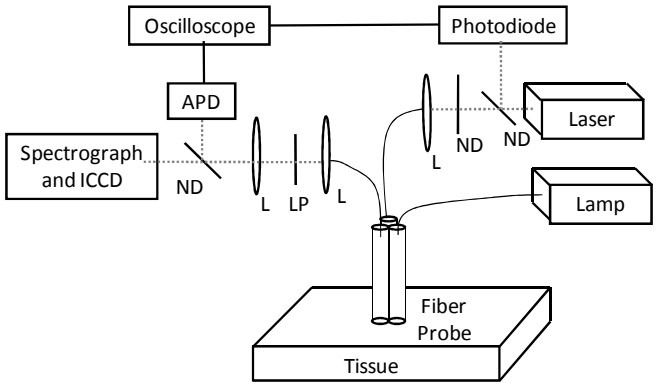

Fig. 1. (a) Schematic of clinical instrumentation. ND = neutral density filter, L = lens, LP = long pass filter, APD = avalanche photodiode, ICCD = intensified charge coupled device.

2.2 Human studies

Reflectance and fluorescence spectra were measured from human pancreatic tissue samples obtained at the U of M Medical Center within 30 minutes of excision, during operative procedures (Whipple procedure or distal pancreatectomy) performed on 9 patients (average age 62 ± 11 years; 7 female, 2 male). In the Whipple procedure, the head and proximal body of the gland were removed, while in the distal pancreatectomy, the tail and a portion of the body were removed. The amount of tissue removed was driven by the location of the tumor and the surgical anatomy for reconstruction purposes. The study received approval from the Institutional Review Board of the U of M Medical School. Prior to data acquisition, written consent was obtained from each patient.

Spectra were measured from 50 pancreatic tissue sites. Immediately following optical measurement, a tissue biopsy was taken from each of these sites and used for histopathologic analysis. Of the 50 sites, 11 were diagnosed by pathology as histologically normal, 22 were diagnosed as chronic pancreatitis (inflammation), and 17 were diagnosed as adenocarcinoma. All pancreatic adenocarcinoma spectra in this study were from patients who had concurrent histologic evidence of chronic pancreatitis in addition to pancreatic adenocarcinoma. Two wavelength-resolved reflectance spectra and two wavelength-resolved fluorescence spectra were taken from each tissue site, except for one adenocarcinoma site, from which only one set of these three measurements was taken.

Two pairs of chronic pancreatitis spectra were excluded because the fluorescence spectra had a signal-to-noise ratio (SNR) of less than 25, where SNR was defined to be the mean

#130269 - $15.00 USD Received 16 Jun 2010; revised 22 Sep 2010; accepted 23 Sep 2010; published 28 Sep 2010

signal at peak fluorescence divided by the standard deviation of the noise in the measured spectrum. Another pair of chronic pancreatitis spectra was excluded because the intensity of the reflectance signal at 550 nm was less than 1/10 of that at 650 nm. The remaining 96 pairs of reflectance and fluorescence spectra (22 pairs of normal spectra, 41 pairs of chronic pancreatitis spectra, 33 pairs of adenocarcinoma spectra) were individually fit using the PTI model.

3. Photon-tissue interaction (PTI) model

3.1 PTI reflectance model and fitting procedure

The PTI model was described in detail previously [15]. Briefly, an empirical model [18] of reflectance $R^{EMP}(\mu_s, \mu_a; \lambda)$ as a function of the tissue scattering coefficient μ_s (related to the nuclear diameter L and nuclear refractive index n_s) and absorption coefficient μ_a (related to the total hemoglobin concentration $[Hb]_{tot}$ and blood oxygen saturation SO_2) was employed to construct a wavelength-resolved scaling factor to transform an average measured "canonical normal" pancreatic tissue reflectance spectrum $R^{MEASURED}{}_{NORMAL}(\mu_a, \mu_s; \lambda)$ into the PTI model spectrum $R^{PTI}{}_{UNKNOWN}(\mu_a, \mu_s; \lambda)$ for each of the 96 individual measured reflectance spectra:

$$R^{PTI}_{UNKNOWN}(\mu_a, \mu_s; \lambda) = \left(R^{MEASURED}_{NORMAL}(\mu_a, \mu_s; \lambda)\right)\left(\frac{R^{EMP}_{UNKNOWN}(\mu_a, \mu_s; \lambda)}{R^{EMP}_{NORMAL}(\mu_a, \mu_s; \lambda)}\right). \quad (1)$$

The PTI-modeled spectra are denoted "unknown" because the model was blinded to pancreatic tissue type. Each model spectrum $R^{PTI}{}_{UNKNOWN}(\mu_a, \mu_s; \lambda)$ resulting from Eq. (1) was individually fit to the corresponding measured reflectance spectrum $R^{MEASURED}(\mu_a, \mu_s; \lambda)$ by varying the nuclear diameter L, total hemoglobin concentration $[Hb]_{tot}$, and blood-oxygen saturation SO_2 over biologically reasonable ranges (Table 1) and minimizing the cost function $|R^{PTI}{}_{UNKNOWN} - R^{MEASURED}|$ over the wavelength range of 400 nm to 700 nm [15].

Table 1. Ranges and step sizes for tissue parameters in the PTI model

Tissue parameter	Minimum value	Maximum value	Step size
L	9 μm	13.5 μm	0.9 μm
$[Hb]_{tot}$	1.1 μM	11 μM	1.1 μM
SO_2	0.1	0.9	0.2

The fitting procedure in this study was identical to that developed in [15], except for five changes: (1) The measured "canonical normal" spectrum was taken to be an average of all 22 measured normal spectra. (Each normal reflectance spectrum was first normalized to its peak value in the 400-700 nm wavelength range, then all 22 of these spectra were averaged, and, finally, the resulting spectrum was normalized to the peak again to create the "canonical normal" spectrum.). (2) The concentration of collagen fibers (cylindrical scatterers) for all unknown reflectance spectra was set to three times that of the canonical normal (motivated by previous work demonstrating that the mean collagen content of both pancreatic cancer and tumor-associated chronic pancreatitis was roughly three times as high as that of normal pancreatic tissue [19]). This approximation was not expected to have a significant effect on the fitting procedure, because the key disease-related changes in the reflectance spectra were expected to be captured by changes in the variable L [15]. (3) The refractive index of cell nuclei for all tissue types was set to a constant value of 1.375, which was in good agreement with previous results [15]. (4) The nuclear diameter L was varied from 9 μm to 13.5 μm, which contains the anticipated range for the pancreatic tissue types examined in this study [20,21]. (5) In the correction factor for the confinement of blood to cylindrical vessels, the absorption coefficient of whole blood [18] was used.

In this way, the parameters extracted from the best fit of each "unknown" reflectance spectrum to the PTI model were the mean diameter L of the cell nuclei, as well as the total

#130269 - $15.00 USD Received 16 Jun 2010; revised 22 Sep 2010; accepted 23 Sep 2010; published 28 Sep 2010

hemoglobin concentration and blood-oxygen saturation. The value of L from each "unknown" reflectance spectrum was compared to the value L_o (set to 9 μm) that had been input into the PTI model for the mean cellular nuclear diameter of the "canonical normal" tissue [15]. The ratio of L/L_o, termed the *nuclear dilation factor*, was calculated for each "unknown" reflectance spectrum. The tissue scattering properties extracted from the PTI model were then employed to correct the corresponding fluorescence spectra for attenuation artifacts, as described in Section 3.2.

3.2 PTI fluorescence model and fitting procedure

Once the model described above was fit to an individual measured reflectance spectrum, the corresponding measured fluorescence spectrum $F_{MEASURED}(\lambda)$ was corrected for scattering and absorption attenuation artifacts with a Beer-Lambert factor [15], where the scattering coefficient was obtained from fitting the reflectance spectrum (Section 3.1). The resulting "intrinsic" fluorescence spectrum $F_{INTRINSIC}(\lambda)$ was fit to a linear combination of the basis spectra from three endogenous tissue fluorophores: extracellular collagen, intracellular NADH, and intracellular FAD, as described previously [15]:

$$F_{INTRINSIC}(\lambda) = C_{COLL}F_{COLL}(\lambda) + C_{NADH}F_{NADH}(\lambda) + C_{FAD}F_{FAD}(\lambda). \qquad (2)$$

The extracted fit coefficients C_{COLL}, C_{NADH}, and C_{FAD} were then normalized via division by their sum, in order to obtain the percentage contributions *%COLL*, *%NADH*, and *%FAD* from the constituent endogenous tissue fluorophores [15]. These percentages summed to 100% for each measured fluorescence spectrum.

4. Results

4.1 Measured reflectance and fluorescence spectra from human pancreatic tissues

Figure 2 shows representative reflectance and fluorescence spectra measured from normal pancreatic tissue, chronic pancreatitis, and pancreatic adenocarcinoma.

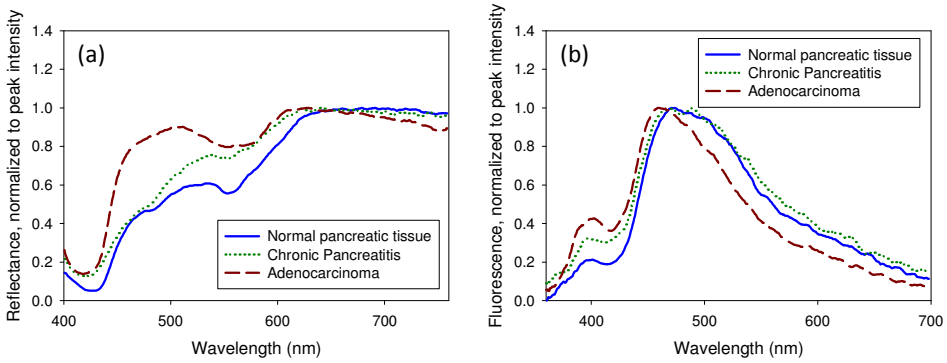

Fig. 2. Representative (a) reflectance and (b) fluorescence spectra of normal pancreatic tissue, chronic pancreatitis, and pancreatic adenocarcinoma.

As reported previously [13–15], there are noticeable differences between the spectra of the different tissue types. From 450 nm to 530 nm, there is a significant increase in the amplitude of the adenocarcinoma reflectance spectrum (relative to normal and chronic pancreatitis), attributed to the increased size of cell nuclei in adenocarcinoma [20,21]. Near 400 nm, there are notable increases in the amplitude of the adenocarcinoma and chronic pancreatitis fluorescence spectra (relative to normal), attributed to the increased extracellular collagen content in adenocarcinoma and chronic pancreatitis [19].

#130269 - $15.00 USD Received 16 Jun 2010; revised 22 Sep 2010; accepted 23 Sep 2010; published 28 Sep 2010

4.2 Fits of PTI model to reflectance and fluorescence spectra

Figure 3 shows best fits of the PTI model to reflectance and fluorescence spectra from chronic pancreatitis and pancreatic adenocarcinoma. The average error in fit of the PTI reflectance model to the 96 measured spectra was less than 16% in the wavelength range 450-530 nm. This spectral range is where significant differences in spectral amplitude were reported for adenocarcinoma, relative to normal pancreatic tissue and pancreatitis [13–15], as can be seen in Fig. 2(a).

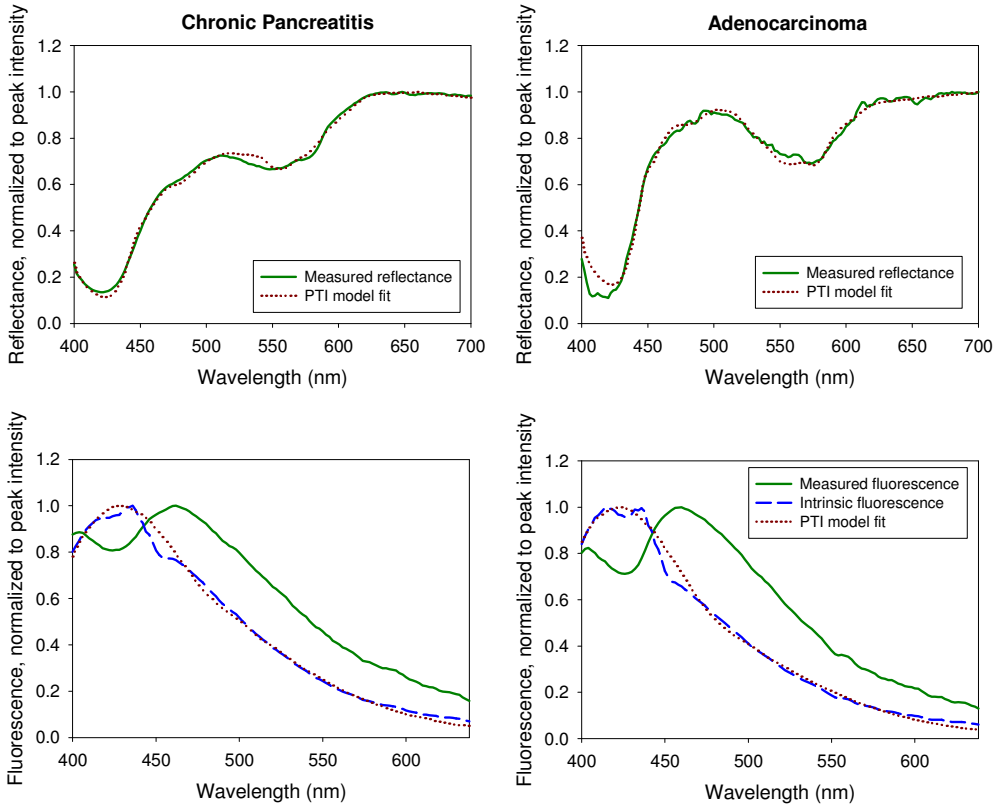

Fig. 3. Best fits of the PTI model to measured reflectance spectra (top row) and intrinsic fluorescence spectra (bottom row) for chronic pancreatitis (left column) and adenocarcinoma spectra (right column). Over all measured spectra, the average error in fit of the PTI reflectance model was less than 16% in the wavelength range 450-530 nm, and the average error in fit of the PTI fluorescence model was less than 6% in the wavelength range of 500-550 nm.

The average error in fit of the PTI fluorescence model to the 96 "intrinsic" fluorescence spectra was less than 6% in the wavelength range of 500-550 nm, in which key differences in spectral amplitude were reported [13–15] for the different pancreatic tissue types (see Fig. 2(b)). When the 11 (out of 96) reflectance spectra with the highest cost functions were discarded, the average error in fit of the PTI reflectance model to the remaining 85 reflectance spectra fell below 10% in the 450-530 nm wavelength range, the average error in fit of the PTI fluorescence model to the 85 corresponding fluorescence spectra in the 500-550 nm wavelength range was nearly unchanged (remaining at less than 6%), and there was no significant change to the mean or standard error for the extracted parameters (see Sections 4.3 and 4.4 below).

#130269 - $15.00 USD Received 16 Jun 2010; revised 22 Sep 2010; accepted 23 Sep 2010; published 28 Sep 2010

4.3 PTI reflectance model extracts cellular nuclear dilation factor

Figure 4 shows the cellular nuclear dilation factor L/L_o extracted from the PTI model for each pancreatic tissue type. The mean ± standard error values of L/L_o extracted for normal pancreatic tissue, chronic pancreatitis, and pancreatic adenocarcinoma were 1.04 ± 0.01, 1.07 ± 0.02, and 1.27 ± 0.01, respectively. The extracted parameter L/L_o can distinguish between adenocarcinoma and normal pancreatic tissue, as well as between adenocarcinoma and chronic pancreatitis ($p < 2\text{x}10^{-9}$ from Wilcoxon rank-sum tests). This result is consistent with the larger average cellular nuclear diameters found in histopathological analysis of pancreatic adenocarcinoma relative to normal pancreatic tissue and chronic pancreatitis [20–22].

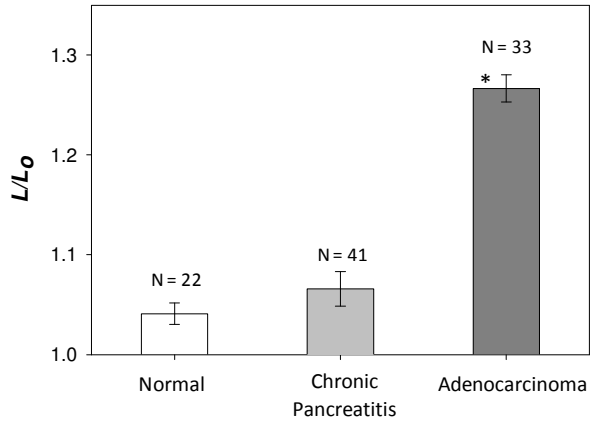

Fig. 4. Extracted nuclear dilation factor L/L_o for normal pancreatic tissue (N = 22 spectra), chronic pancreatitis (N = 41 spectra), and pancreatic adenocarcinoma (N = 33 spectra). Differences were statistically significant (*, $p < 2\text{x}10^{-9}$ from Wilcoxon rank-sum tests) for distinguishing adenocarcinoma from normal pancreatic tissue as well as distinguishing adenocarcinoma from chronic pancreatitis.

4.4 PTI fluorescence model extracts percent contribution of extracellular collagen to intrinsic fluorescence

Figure 5 shows the percentage contribution of extracellular collagen to the intrinsic fluorescence of normal pancreatic tissue, chronic pancreatitis, and pancreatic adenocarcinoma. The mean ± standard error values of the percent contributions of extracellular collagen fluorescence to the spectra of normal pancreatic tissue, pancreatitis, and adenocarcinoma were 15.1 ± 3.4, 29.5 ± 3.8, and 60.9 ± 4.8, respectively. The results shown in Fig. 5 suggest that the percentage contribution of extracellular collagen to the intrinsic fluorescence is potentially useful (*, $p < 2\text{x}10^{-5}$ from Wilcoxon rank-sum tests) for distinguishing adenocarcinoma from normal pancreatic tissue, as well as distinguishing adenocarcinoma from chronic pancreatitis. Figure 5 also shows that the percentage contribution of extracellular collagen to the intrinsic fluorescence is potentially useful (**, $p < 3\text{x}10^{-2}$ from Wilcoxon rank-sum test) for distinguishing chronic pancreatitis from normal pancreatic tissue. These results agree with qualitative histopathological observation [15,23] and hydroxyproline content analysis [19], both of which have revealed increases in the amount of collagen found in chronic pancreatitis and pancreatic adenocarcinoma, relative to normal pancreatic tissue.

#130269 - $15.00 USD Received 16 Jun 2010; revised 22 Sep 2010; accepted 23 Sep 2010; published 28 Sep 2010

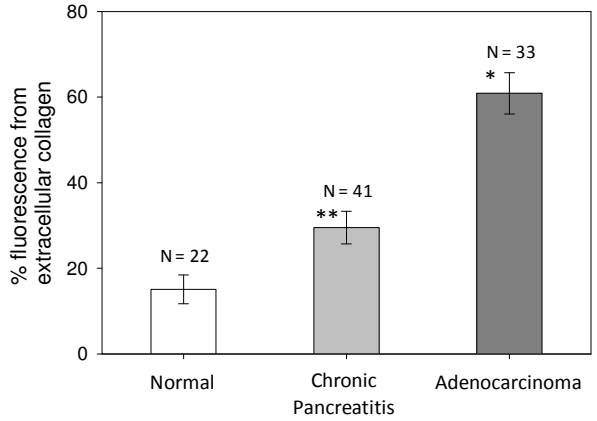

Fig. 5. Extracted percentage contributions of extracellular collagen to intrinsic fluorescence spectra of normal pancreatic tissue (N = 22 spectra), chronic pancreatitis (N = 41 spectra), and pancreatic adenocarcinoma (N = 33 spectra). Differences were statistically significant for distinguishing adenocarcinoma from normal pancreatic tissue as well as distinguishing adenocarcinoma from chronic pancreatitis (*, $p < 2\text{x}10^{-5}$ from Wilcoxon rank-sum tests). Differences were also statistically significant for distinguishing chronic pancreatitis from normal pancreatic tissue (**, $p < 3\text{x}10^{-2}$ from Wilcoxon rank-sum test).

5. Discussion

The results shown in Figs. 3 and 4 suggest that reflectance and fluorescence spectrocopies have the potential to distinguish among pancreatic tissue types, including normal pancreatic tissues, chronic pancreatitis, and pancreatic adenocarcinoma, using biophysical tissue parameters extracted from the data via the PTI model of light propagation. The relevant biophysical parameters for distinguishing the different pancreatic tissue types were the nuclear dilation factor L/L_o and the percentage contribution of extracellular collagen to the intrinsic fluorescence. The observed increase in the nuclear dilation factor L/L_o for adenocarcinoma, relative to normal pancreatic tissue and chronic pancreatitis, is in agreement with the findings of histopathology that the mean cellular nuclear diameter is larger in pancreatic adenocarcinoma than in normal pancreatic tissue [20] and chronic pancreatitis [21]. The increased percentage contributions of extracellular collagen to the intrinsic fluorescence for adenocarcinoma and chronic pancreatitis (relative to normal pancreatic tissue) are in agreement with studies demonstrating that there is increased collagen content in both pancreatic adenocarcinoma and tumor-associated chronic pancreatitis, relative to normal pancreatic tissue [19]. The increase in collagen content in chronic pancreatitis and adenocarcinoma is due to an increased fibrosis in response to inflammation. In chronic pancreatitis, the chronic inflammation incites chronic and/or recurrent tissue injury, which then heals with scar (fibrosis). In adenocarcinoma, the tumor induces desmoplasia, a stromal response that results in proliferation of mesenchymal cells and production of extracellular collagen.

We note that since different source fibers were used for reflectance and fluorescence measurements, the light paths of the detected reflectance and fluorescence photons likely interrogated slightly different regions of each tissue site. However, since the reflectance and fluorescence photons were both collected by the same detector fiber, and all three fibers were positioned adjacent to each other in a triangular geometry, we used Monte Carlo simulations [24–26] to estimate that the majority of reflectance and fluorescence photons collected at a given tissue site visited roughly the same (~1 mm^3) region of tissue.

The PTI model reported here does not make use of the hemoglobin concentration and blood-oxygen saturation parameters extracted from the reflectance fits. Since the measurements used for training the PTI model in this study were all obtained *ex vivo*, much of

#130269 - $15.00 USD Received 16 Jun 2010; revised 22 Sep 2010; accepted 23 Sep 2010; published 28 Sep 2010

the hemoglobin absorption information obtained from these measurements is likely most directly related to the amount of blood that drained from each tissue sample and the time that each sample was exposed to air prior to measurement. We note that the blood absorption features present in the measured reflectance spectra were likely similar for measurements made on patients who underwent either type of pancreatic surgery (Whipple procedure or distal pancreatectomy). This is a reasonable assumption because in the distal pancreatectomy procedure, the splenic artery was divided early, producing a level of ischemia that was likely similar to that associated with the Whipple surgery.

In an *in vivo* setting, we expect to see changes in the measured reflectance spectra that can be linked to differences in the vasculature and blood oxygenation (and hence, the hemoglobin absorption) of pancreatic adenocarcinoma, chronic pancreatitis, and normal pancreatic tissue [27,28]. We also expect the PTI model to be capable of describing these changes in terms of the total hemoglobin concentration, blood-oxygen saturation, and mean blood vessel radius, as well as the possible addition of a variable to represent the packaging of hemoglobin into erythrocytes [29]. In preparation for future *in vivo* studies, we are working to further refine the PTI model and examine in greater detail the effect of the hemoglobin absorption parameters on the modeled reflectance. We do not anticipate that the accuracy of the PTI model will be significantly affected by the transition to an *in vivo* setting, since the model can account for increased levels of absorption due to blood. Thus, the results reported in this study illustrate the potential of the PTI model to address the clinical need for accurate detection of pancreatic adenocarcinoma in the setting of chronic pancreatitis. An optical sensing technique involving the PTI model could potentially be employed in a clinical setting to guide EUS-FNA biopsy.

6. Conclusions

In this study, we demonstrate the first-ever use of a photon-tissue interaction (PTI) model to fit individual reflectance and fluorescence spectra from human pancreatic tissues. The best fits of the PTI model to the optical spectra extracted diagnostically-relevant biophysical parameters. The nuclear dilation factor was extracted from the PTI reflectance model, and the percent contribution of extracellular collagen to the intrinsic fluorescence was extracted from the PTI fluorescence model. Both of these parameters were statistically significant for distinguishing pancreatic adenocarcinoma from normal pancreatic tissue, as well as for distinguishing adenocarcinoma from chronic pancreatitis. Furthermore, the percent contribution of extracellular collagen to the intrinsic fluorescence was also statistically significant for distinguishing chronic pancreatitis from normal pancreatic tissue. These results indicate that optical spectroscopy involving a photon-tissue interaction model has the potential to quantitatively distinguish between different pancreatic tissue types and to provide an inroad toward addressing the clinical need for accurate detection of early-stage pancreatic cancer.

Acknowledgements

This work was supported in part by the National Institutes of Health (NIH-CA-114542), the National Pancreas Foundation, the Wallace H. Coulter Foundation, the U of M Comprehensive Cancer Center, and a grant from the U of M Medical School Translational Research Program. We thank Drs. C. Sonnenday and L. M. Colletti for permitting us to collect data during pancreatic surgeries that they performed. We also thank Emma Salomonsson for assistance with background research.

#130269 - $15.00 USD Received 16 Jun 2010; revised 22 Sep 2010; accepted 23 Sep 2010; published 28 Sep 2010